Nano Materials Science xxx (xxxx) xxx

Contents lists available at ScienceDirect

Nano Materials Science

journal homepage: www.keaipublishing.com/cn/journals/nano-materials-science/

Facile synthesis of zinc-based organic framework for aqueous Hg (II) removal: Adsorption performance and mechanism

Biao Zeng [a,b], Wei Wang [a,b], Sijin He [c], Guo Lin [a,b,*], Wenjia Du [d], Jun Chang [e], Zhao Ding [a,f,**]

[a] The State Key Laboratory of Refractories and Metallurgy, Wuhan University of Science and Technology, Wuhan, 430081, PR China
[b] Key Laboratory for Ferrous Metallurgy and Resources Utilization of Ministry of Education, Wuhan University of Science and Technology, Wuhan, 430081, PR China
[c] China E-port Data Center Division of Chengdu, Chengdu, 610041, PR China
[d] Electrochemical Innovation Lab, Department of Chemical Engineering, University College London (UCL), London, WC1E 6BT, UK
[e] College of Material and Chemical Engineering, Tongren University, Tongren, 554300, Guizhou, PR China
[f] Department of Mechanical, Materials and Aerospace Engineering, Illinois Institute of Technology, Chicago, IL, 60616, USA

ARTICLE INFO

Keywords:
Metal-organic frameworks (MOFs)
Hg (II)
Selectivity
Adsorption mechanism

ABSTRACT

Mercury (Hg) ions can lead to a serious impact on the environment; therefore, it was necessary to find an effective method for absorbing these toxic Hg ions. Here, the adsorbent (Zn-AHMT) was synthesized from zinc nitrate and 4-amino-3-hydrazine-5-mercapto-1,2, 4-triazole (AHMT) by one-step method and, characterized the microstructure and absorption performance by fourier transform infrared spectroscopy (FTIR), field emission scanning electron microscopy (FESEM), X-ray diffraction (XRD), Brunauer-Emmett-Teller (BET), Thermal Gravimetric Analyzer (TGA) and X-ray photoelectron spectroscopy (XPS). Through a plethora of measurements, we found that the maximum adsorption capacity was 802.8 mg/g when the optimal pH of Zn-AHMT was 3.0. The isothermal and kinetic experiments confirm that the reaction process of Zn-AHMT was chemisorption, while the adsorption process conforms to the Hill model and pseudo second order kinetic model. Thermodynamic experiments showed that the adsorption process was spontaneous and exothermic. Selective experiments were performed in the simulated wastewater containing Mn, Mg, Cr, Al, Co, Ni, Hg ions. Our results showed that the Zn-AHMT has a stronger affinity for Hg ions. The removal rate of Zn-AHMT remained above 98%, indicating that the Zn-AHMT had a good stability validated by three adsorption-desorption repeatable tests. According to the XPS results, the adsorption reaction of Zn-AHMT was mainly attributed to the chelation and ion exchange. This was further explained by both density functional theory (DFT) calculation and frontier molecular orbital theory. We therefore propose the adsorption mechanism of Zn-AHMT. The adsorption reaction facilitates via the synergistic action of S and N atoms. Moreover, the bonding between the adsorbent and the N atom has been proved to be more stable. Our study demonstrated that Zn-AHMT had a promising application prospect in mercury removal.

1. Introduction

Environmental issues have posed a threat to the human society and attracted research attentions in recent years. With the worsening of environmental pollution, it is urgently need to strengthen environmental treatment by novel technologies. The heavy metal pollution is one of the most challenging issues in environmental governance because of its high toxicity and easy accumulation [1]. Among the numerous heavy metals (such as Ni, Cr, Hg, As, Pb, etc), mercury has received extensive attention. According to Huang et al., the forms of mercury mainly include inorganic mercury and organic mercury [2]. Inorganic mercury is mainly produced in the process of agriculture, electronic production, metallurgy, etc., which can cause deafness, blindness, mental disorder, paralysis and other hazards to human beings. Furthermore, inorganic mercury can be transformed into more toxic organic mercury through the action of methanogens and other bacteria, which mainly causes serious damage to human nerves and brain [2–4]. Hence, it is crucial to reduce the mercury pollution by effective treatment of inorganic mercury. Mercury ions are the main form of inorganic mercury, which is one of the most toxic heavy metals and can cause harm to humans at very low concentrations [5]. Therefore, many organizations have made regulations regarding mercury ion concentration. For example, the World Health Organization (WHO)

* Corresponding author. The State Key Laboratory of Refractories and Metallurgy, Wuhan University of Science and Technology, Wuhan, 430081, PR China.
** Corresponding author. The State Key Laboratory of Refractories and Metallurgy, Wuhan University of Science and Technology, Wuhan, 430081, PR China.
E-mail addresses: linguo@wust.edu.cn (G. Lin), zhaoding@wust.edu.cn (Z. Ding).

https://doi.org/10.1016/j.nanoms.2021.06.005

Available online xxxx

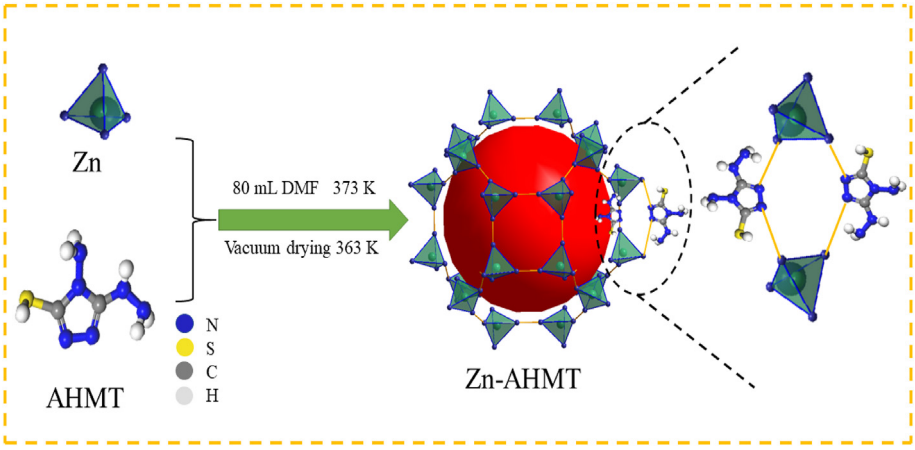

Scheme 1. The synthesis process of the Zn-AHMT.

states that the concentration of mercury ions in drinking water should be less than $1\mu g/L$ [6]. And the standard of the U.S. EPA is a mercury level of 2 mg/L [7].

There are some traditional techniques for removing mercury ions from wastewater, such as precipitation, adsorption, membrane separation and ion exchange and so on [1,8–10]. Among these technologies, adsorption method is widely used because of its low cost, simple operation and no secondary pollution [11]. Recently, numerous adsorbents have been developed to remove mercury ions from water. The typical adsorbents include activated carbon, zeolite, chitosan and clay materials [12–14]. Mokhtari et al. used modified activated carbon to adsorb mercury ions in aqueous solution, and the maximum adsorption capacity reached 377.68 mg/g under the optimal conditions. However, the disadvantage of the adsorbent is poor selectivity [15]. Donia et al. reported the magnetic chitosan resin can selectively adsorb mercury ions, but the adsorption amount is low, only 2.8 mmol/g [16]. Hence, to improve the absorption capabilities, it is necessary to develop a new adsorbent to make up for these deficiencies.

Recently, metal-organic frameworks (MOFs) have attracted the considerable attentions. MOFs are crystal structures composed of metal clusters and organic ligands [17]. It is widely used in catalysis, gas storage, separation and other fields [18–23] because of its advantages of uniform pore structure, stable chemical properties, functionalization and simple preparation process [22,24–26]. Also, it has been found that MOFs have great potential in the field of wastewater treatment. Luo et al. used functionalized MIL-101(Cr) to selectively remove lead in the solution with multiple ions coexisting, but the adsorption capacity was only 81.09 mg/g [27]. Jiang et al. reported that ZIF-8 could efficiently adsorb trivalent rare earth element La from aqueous solution, with an adsorption capacity of 385 mg/g. However, the stability of ZIF-8 was not very great since the adsorption capacity reduced from 385 mg/g to 150 mg/g after three adsorption-desorption processes [28]. MOFs materials still need to be improved in open literatures. Therefore, many scholars have tried to either modify and functionalize MOFs or improve these deficiencies through other technologies. Chang et al. used an amino-modified zirconium-based MOF (UIO-66-NH2) to adsorb Au (III) from solution, and the adsorption capacity could reach 650 mg/g [29]. The stability and selectivity of this adsorbent showed promising results. Besides, the adsorption capacities of functionalized Zn-MOF prepared by Huang et al. reached 1097 mg/g and 718 mg/g for Pb and As at pH was 4 and 6, respectively [30]. Nevertheless, this study is based upon the experience of predecessors, and we prepared an efficient MOFs adsorbent for the removal of mercury ions in wastewater.

In this study, the one-step method was used to directly synthesize the adsorbents (Zn-AHMT) using the zinc nitrate and 4-amino-3-hydrazino-5-mercapto-1, 2, 4-triazole (AHMT). The optimum pH of Zn-AHMT was determined by setting mercury solution with different pH. The selectivity and reproducibility experiments of Zn-AHMT were performed. Also, the adsorption capacity of Zn-AHMT at different time and initial ion concentration was investigated. In addition, the state of Zn-AHMT before and after adsorption was characterized by BET, XRD, XPS, SEM-EDS, and FTIR. To strengthen the credibility of high absorption, we further analyzed the adsorption of Zn-AHMT by performing a series of measurements, including the adsorption kinetics, isotherm, thermodynamics, density functional theory (DFT) calculation and frontier analytical orbital theory. Our results demonstrated that the synthesized Zn-AHMT can effectively remove Hg ions from wastewater.

2. Experiments and methods

2.1. Materials

Zinc nitrate hexahydrate was purchased from Tianjin Beilian Fine Chemicals Development Co., Ltd., 4-amino-3-hydrazino-5-mercapto-1,2,4-triazole was purchased from Aladdin Co., Ltd. N, N-Dimethylformamide (DMF) and ethanol absolute were purchased from Sinopharm Group Chemical Reagent Co. Ltd. Mercury standard solution ($1000\ \mu g/mL$) was purchased from National Nonferrous Metals and Electronic Materials Analysis and Testing Center. Deionized water was purchased from Red Wilderness. Thiourea was produced in Sinopharm Group Chemical Reagent Co. Ltd. Throughout the experiment, sodium hydroxide and nitric acid (analytical grade) were used to adjust the pH of the solution. Wastewater (Hg^{2+}, Ni^{2+}, Co^{2+}, Mg^{2+}, Mn^{2+}, Al^{3+}, Cr^{3+}) was simulated wastewater in the laboratory.

2.2. Preparation of adsorbent

Firstly, 3 g of zinc nitrate and 1.3 g of 4-amino-3-hydrazino-5-mercapto-1, 2, 4-triazole were added to a 250 mL three-necked flask. Then, 80 mL of DMF and 1 mL of hydrochloric acid were added to the three-necked flask. After the solids were dissolved, condensation reflux was carried out at 373 K for 24 h. Finally, the products obtained after the reaction were washed three times with DMF, deionized water and ethanol solution respectively, and then dried in a vacuum drying oven at 363 K for 24 h to obtain the experimental sample, termed as Zn-AHMT. The synthesis process of Zn-AHMT was shown in Scheme 1.

2.3. Adsorption experiments

In order to determine the optimal pH of Zn-AHMT in the adsorption experiment, the pH of mercury solution was set to 1.0–7.0 in this experiment.10 mg of Zn-AHMT and 15 mL of 100 mg/L were placed in a 15 mL centrifuge tube and oscillated (200 rpm) for 24 h at room temperature. Then, the solution was filtered to obtain the supernatant, and

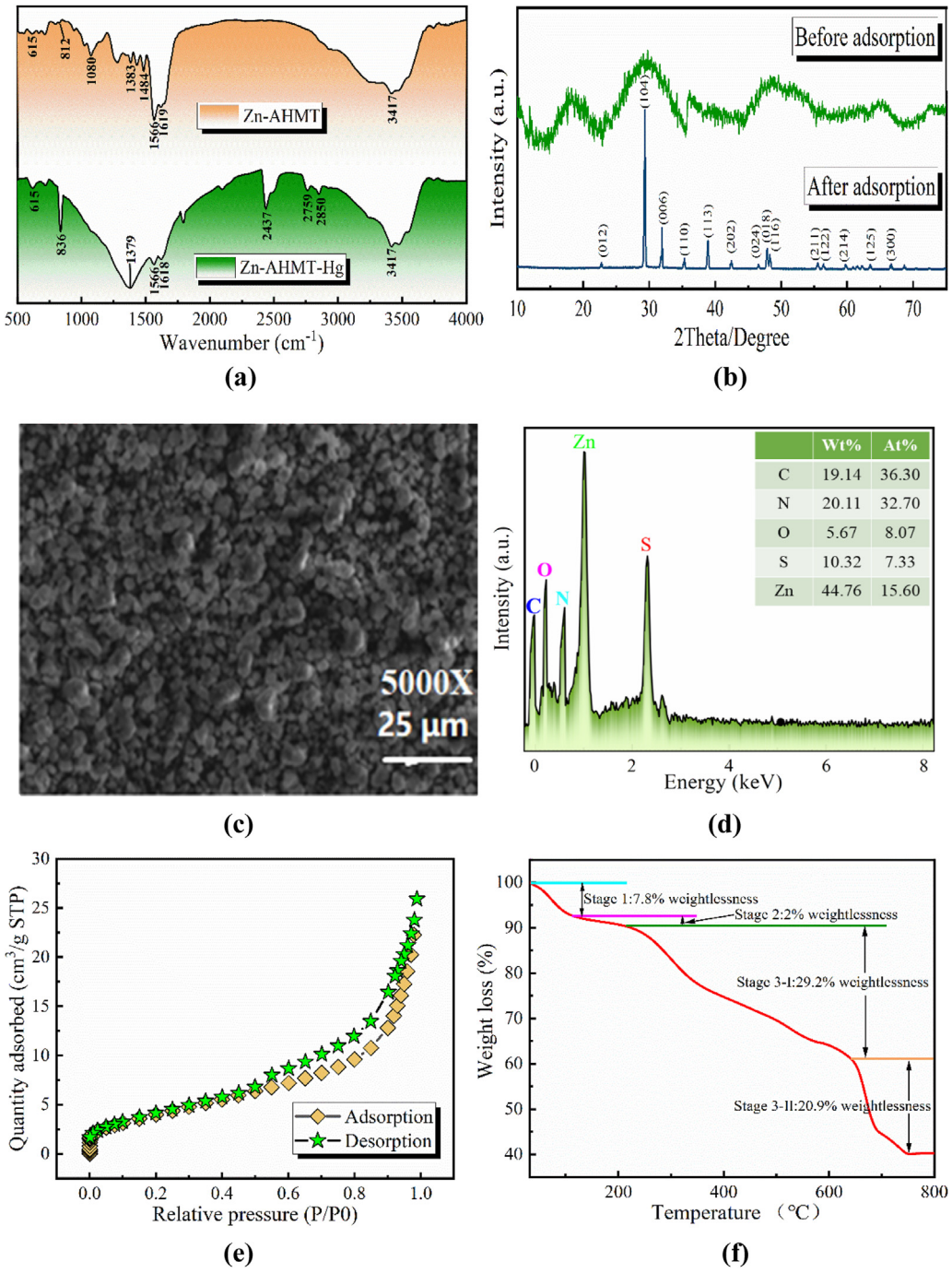

Fig. 1. FTIR spectra (a), XRD patterns (b), FESEM image (c), EDS (d), N2 absorption-desorption isotherm (e), the thermogravimetric analyze (f) of Zn-AHMT.

the inductively coupled plasma mass spectrometry (ICP-MS) was used to determine the concentration of residual mercury ions in supernatant.

To investigate the effect of time on adsorption capacity, 10 mg of Zn-AHMT and 10 mL of 10 mg/L mercury solution were added to a 15 mL centrifuge tube and oscillated (200 rpm) for 10, 20, 30, 60, 120, 240, 420 min at room temperature, respectively.

To explore the influence of initial concentration of mercury ions on adsorption capacity, mercury solution was set at 100, 200, 300, 400, 500, 600 mg/L, respectively. Then 10 mg of Zn-AHMT and 30 mL of mercury solution were placed in a 50 mL centrifuge tube and oscillated (200 rpm) for 24 h at room temperature.

In order to investigate whether the adsorption process of Zn-AHMT was endothermic or exothermic, 10 mg of Zn-AHMT and 15 mL of mercury solution (100 mg/L) reacted for 24 h at 298 K, 308 K and 318 K, respectively.

In the selectivity experiment, 10 mg of Zn-AHMT and 10 mL of laboratory wastewater were added into a 15 mL centrifuge tube and oscillated (200 rpm) at room temperature for 24 h to observe the changes in the concentration of ions before and after adsorption.

In the repeatability experiment, 40 mg of Zn-AHMT and 40 mL of mercury solution were added to a 50 mL centrifuge tube and oscillated (200 rpm) at room temperature for 24 h. Then took the supernatant to measure the concentration of mercury ions, and then added the same amount of thiourea solution (10 %) to the reaction solid, oscillating (200 rpm) at room temperature for 24 h. Followed the above steps and repeated the operation for 5 times to complete the repeatability

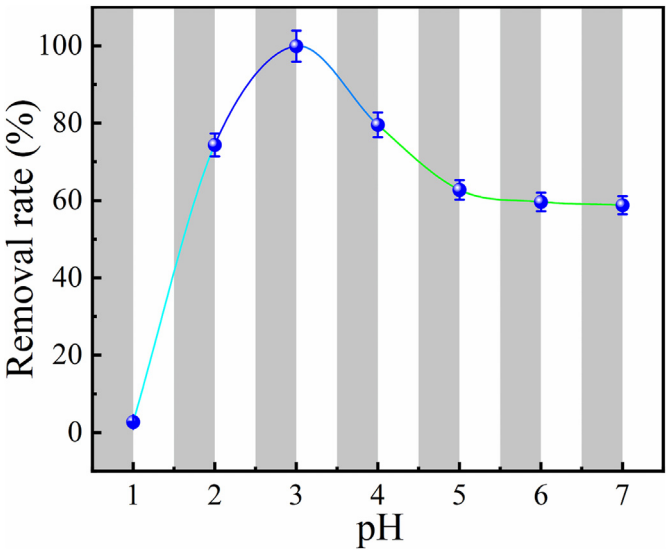

Fig. 2. Effect of pH on removal rate of mercury ions.

experiment.

The relevant calculation formula was as follows (1)–(2):

$$R = \frac{(C_0 - C_e)}{C_0} \times 100\% \quad (1)$$

$$Q_e = \frac{(C_0 - C_e) \times V}{W} \quad (2)$$

Where R is the adsorption rate (%), Q_e is the adsorption amount at equilibrium (mg/g), C_0 is the initial concentration of the solution (mg/L), and C_e is the equilibrium concentration of the solution (mg/L), V represents the volume of the solution (mL) and W represents the mass of Zn-AHMT (mg).

3. Results and discussion

3.1. Characterization

To determine whether Zn-AHMT was successfully synthesized, and to analyze the morphology and structure of Zn-AHMT, the synthesized products were characterized by FTIR, XRD, SEM-EDS and BET. The FTIR spectra of Zn-AHMT and Zn-AHMT-Hg were shown in Fig. 1(a). The 1st peak at 615 cm^{-1} was due to the stretching vibration of C-S [31]. A weak peak appeared at 812 cm^{-1}, which might be caused by Zn-N [32], suggesting that the zinc base and organic ligand were bound together. The peak at 1383 cm^{-1} was attributed to the stretching vibration of C-N [33]. According to the reported of Peng and Qiu et al., the peaks at 1484 cm^{-1} and 1566 cm^{-1} belong to C=N [1,34]. Next, the peaks at 1619 cm^{-1} and

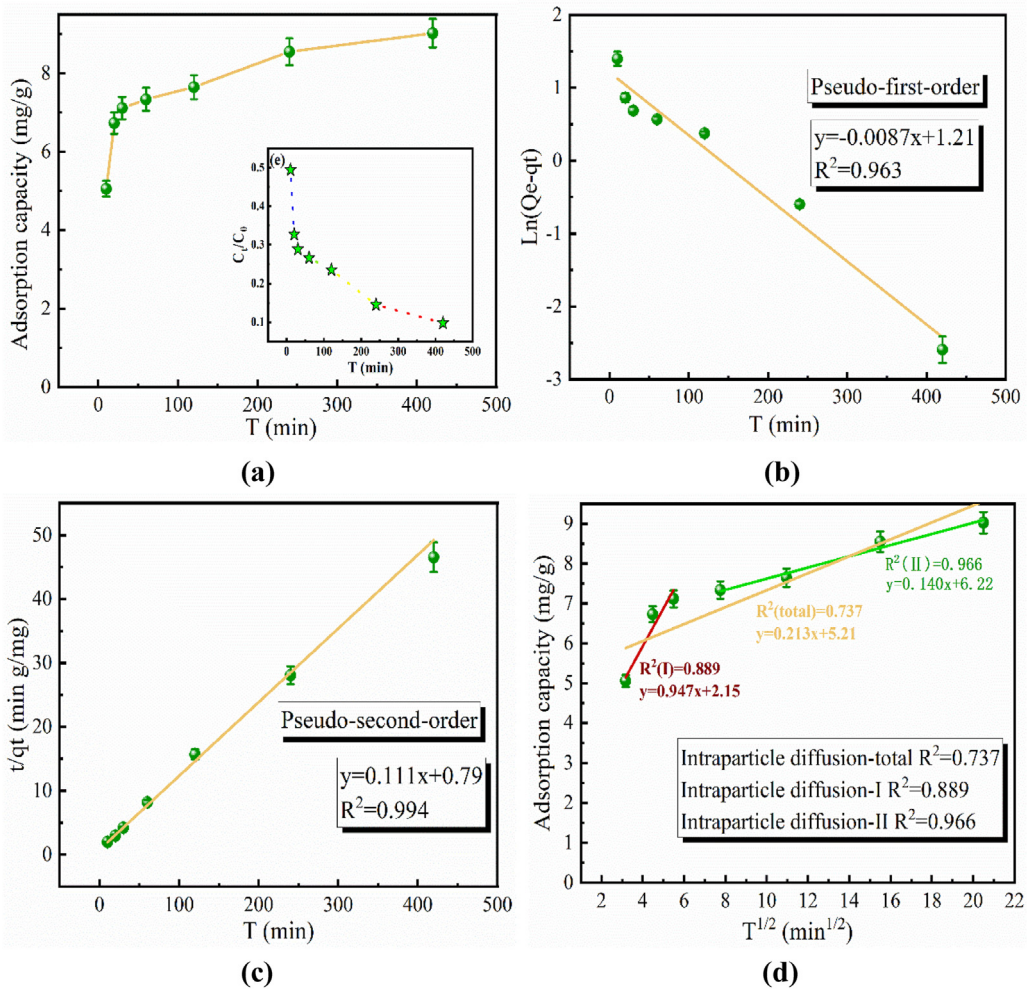

Fig. 3. Effect of time on adsorption capacity (a), linear fit with the PFO model (b), PSO model (c), and ID model (d) for Hg (II) adsorption onto Zn-AHMT, adsorption rate of Hg (II) on Zn-AHMT.

3417 cm^{-1} were correspond to -NH_2 [35] and N-H [1], respectively. After adsorbing Hg (II), it was obvious to observe that the stretching vibration peak of Zn-N was shifted from 812 cm to 1 to 836 cm-1 and, the C-N peak was shifted from 1383 cm to 1 to 1379 cm-1. Above results confirm that Zn-AHMT specimen was successfully synthesized with a stable chemical structure before and after adsorption.

As shown in Fig. 1(b), the XRD patterns of after adsorbing Hg (II), multiple sharp characteristic peaks appeared at (012), (104), (006), (100), (113), (202), (024), (018), (116), (211), (122), (214), (125) and (300), indicating that the Zn-AHMT combined with mercury ions had a good crystal structure compared with before mercury absorption. According to the SEM pattern (Fig. 1(c)) of Zn-AHMT, it could be seen that the adsorbent was uniformly distributed in granular form. The EDS pattern showed (Fig. 1(d)) the chemical composition (C, N, O, S, Zn) of Zn-AHMT and listed the atomic and mass ratios of each element. And the presence of Zn, S, N elements in pattern also indicated that Zn-AHMT was successfully synthesized. To study the specific surface area and pore volume of Zn-AHMT, BET and N_2 adsorption-desorption isotherms were used in this experiment. The specific surface area, pore volume and average pore diameter of Zn-AHMT were 15.37 m^2/g, 0.032 cm^3/g and 10.59 nm respectively as shown in Fig. 1(e).

The thermogravimetric analysis of Zn-AHMT was shown in Fig. 1(f), from which it could be seen that in the first stage, the mass loss of 7.8% when the temperature rose from room temperature to 115 °C was due to the loss of residual water and other solvents in the adsorbent channel as the temperature rose during the heating process. The temperature of the second stage was between 115 °C and 213 °C, and the mass loss in this process was only 2%. It could be considered that Zn-AHMT could exist stably in this temperature range. The weightlessness of the third stage was mainly after 213 °C. The total weightlessness of this stage is 51%, including 29.2% of stage-I and 20.9% of stage-II respectively. From this stage, the skeleton structure of the adsorbent was gradually destroyed.

3.2. Effect of pH on Hg^{2+} removal

pH was a vital and essential factor affecting the removal efficiency of Zn-AHMT. In Fig. 2, when the pH was 1.0–3.0, the removal rate of Zn-AHMT significantly increased, while the removal rate gradually decreased when the pH was 3.0–7.0, indicating that pH=3.0 was the optimal pH for removing mercury ions, and the removal rate reached at 99.91%. When the pH was 1.0, the removal rate was only 2.7%, this is because at low pH the amino and sulfhydryl functional groups on Zn-AHMT were protonated, resulting in a large repulsive force of Zn-AHMT to Hg^{2+}, thus reducing the removal rate of Zn-AHMT. There were a large number of active sites on the surface of Zn-AHMT to adsorb Hg^{2+}, and the amino, sulfhydryl and other nitrogen-containing groups to Hg^{2+} strong binding force, so when the pH was 1.0–3.0, Zn-AHMT was deprotonated, the removal rate increased as the active sites were occupied. As pH continued to increase, Hg^{2+} would undergo hydrolysis reaction, and Hg $(OH)^+$, Hg $(OH)_2$, Hg $(OH)_3^-$, and Hg $(OH)_4^{2-}$ would be generated in the solution. Since these hydrolyzed products would not be adsorbed by Zn-AHMT, the removal rate thus gradually decreases. Through the above analysis, it could be seen that Zn-AHMT could achieve a better removal effect of mercury ions under acidic conditions.

3.3. Effect of time on adsorption capacity

The influence of time on adsorption capacity was also one of the important factors to be considered in the experimental process. The experimental results were shown in Fig. 3(a) and the adsorption rate of Hg (II) on Zn-AHMT was displayed in Fig. 3(e). It could be seen that the adsorption rate and the adsorption amount increased sharply with time during the period of 10–30 min, because there were a large number of adsorption sites on the surface of the adsorbent at the initial stage of adsorption, which could effectively adsorbed mercury ions. As time gone on, the adsorption sites were gradually occupied, so after 240 min, the adsorption rate decreased and the adsorption capacity changed significantly slowly with time, and the adsorption equilibrium could be achieved after 420 min. In order to further explore the adsorption mechanism of the adsorbent, the pseudo-first order, pseudo-second order and intra particle diffusion models were used to study the adsorption process. The pseudo-first order (PFO) assumed adsorption process to be controlled by penetration and introduced the penetration as the determining step, and the pseudo-second order (PSO) assumed the adsorption process was chemical reactions [36,37]. Intraparticle diffusion (ID) was a multi-process adsorption process, which could be divided into three stages: film diffusion, intraparticle diffusion and mass action [38]. Since the full diffusion occurred in a short period of time, two-stage fitting was carried out for the data in this work. The linear fitting results based on the experimental data were shown in Fig. 3(b–d), and the corresponding experimental parameters were listed in Table 1. The linear fitting formula was shown in Formula S1.

Table 1
Kinetic model parameters.

Kinetic models	Parameters	Value
Pseudo-first order	Q_e (mg/g)	9.112
	K_1 (1/min)	-0.0087
	R^2_{adj}	0.963
Pseudo-second order	Q_e (mg/g)	9.082
	K_2 (g/mgδmin)	0.111
	R^2_{adj}	0.994
Intraparticle diffusion-total	K_3 (g/mg$\delta$$min^{1/2}$)	0.213
	R^2_{adj}	0.737
Intraparticle diffusion-I	$K_{3\text{-}I}$ (g/mg$\delta$$min^{1/2}$)	0.947
	R^2_{adj}	0.889
Intraparticle diffusion-II	$K_{3\text{-}II}$ (g/mg$\delta$$min^{1/2}$)	0.140
	R^2_{adj}	0.966

Through the comparative analysis of the results, it was known that R^2(PSO)=0.994> R^2(PFO)=0.963, and the calculated theoretical value (Q_e=9.082 mg/g) was very close to the actual value (Q_e=9.025 mg/g) obtained from the experiment. Therefore, it could be considered that the adsorption process of Zn-AHMT conform to the pseudo-second order model, which was a chemical adsorption process. Intraparticle diffusion further explained the adsorption mechanism, and the fitting results showed that $K_{3\text{-}II}$=0.966> $K_{3\text{-}I}$=0.889, indicating that the process was mass action, which was the result of the interaction between the active site on the surface of Zn-AHMT and mercury ions.

3.4. Effect of initial concentration of mercury ions on adsorption capacity

The adsorption isotherm described the adsorption capacity of the adsorbent at different initial concentrations of Hg (II). As could be seen from Fig. 4(a), the adsorption capacity of the adsorbent gradually increased with the increase of Hg (II) concentration, and then reached equilibrium, with the maximum adsorption capacity of 802.8 mg/g. There were a large number of adsorption sites on the surface of the adsorbent. When the concentration was low, a large number of active sites that could bind to Hg (II). However, as the concentration increased, the active sites were occupied and no longer bind to Hg (II), so the adsorption equilibrium was reached. Zn-AHMT and previously reported adsorbents for adsorbing Hg (II) were listed in Table 2. Through the comparison of the maximum adsorption capacity, it was found that the adsorption capacity of Zn-AHMT to Hg (II) was considerable. In addition, in order to understand the adsorption process, four adsorption isotherm models (Langmuir, Freundlich, Temkin, Hill) were used to fit the experimental data, and according to the fitting results, it could be concluded which adsorption method was more favorable for the adsorbent to bind to Hg (II). The corresponding calculation formula was expressed as Formula S2 [39–41].

According to the calculation formula, the corresponding fitting results and experimental parameters were shown in Fig. 4(b) and Table 3, respectively. Due to R^2_{Hill}=0.997>R^2_{Temkin}=0.967>$R^2_{Langmuir}$=0.953>R^2

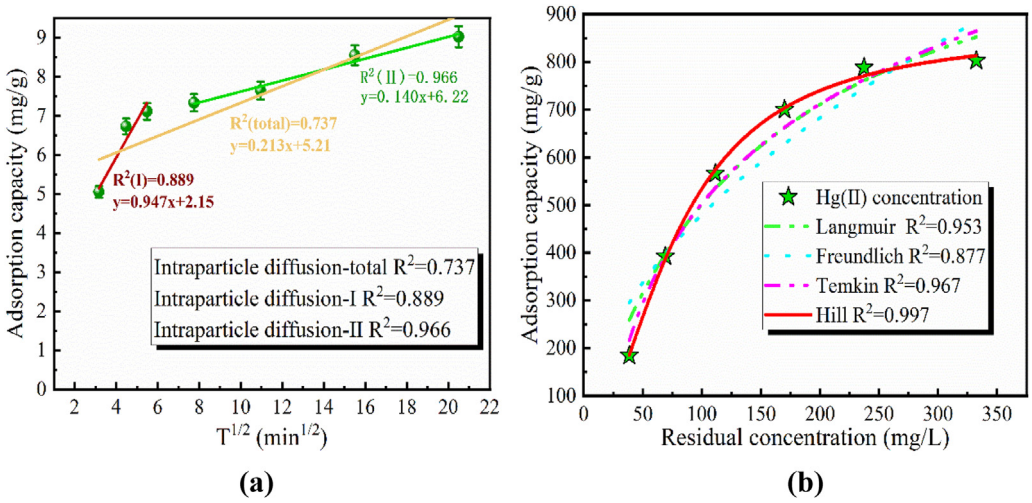

Fig. 4. Effect of the initial concentration of Hg (II) (a), Langmuir, Freundlich, Temkin and Hill model (b).

Table 2
Comparison of adsorption capacity for Hg (II) with adsorbents in literature.

adsorbent	Equilibrium adsorption capacity (mg/g)	References
PAF-1-SH	1000	[43]
SMP	595.2	[44]
Bi-I-functionalized Fe3O4@SiO2@HKUST	264	[22]
MIL-101-Thymine	51.27	[45]
SiO2-CNT	163.9	[46]
CCHLs-DMTD	707	[33]
CCD	116.2	[47]
GO/L-cystine	79.36	[48]
Zn-AHMT	802.8	This work

$_{Freundlich}$=0.887, the adsorption process of Zn-AHMT conformed to the Hill model, indicating that the adsorption process was a multi-molecule chemisorption [31]. The m value of the Hill model was 1.855, indicating that each adsorption site on the adsorbent could adsorb 1.855 Hg (II). In addition, the theoretical adsorption capacity of Hill model was 846.1 mg/g, which was close to the actual adsorption capacity of 802.8 mg/g, indicating that Hill model was suitable to describe the adsorption process.

The dimensionless factor R_A derived from the Langmuir isotherm model was used to study the viability of Zn-AHMT. The formula for R_A was as follows (3) [42]:

$$R_A = \frac{1}{1 + K_A C_0} \quad (3)$$

Table 3
Isothermal model parameters.

Isotherm model	Parameter	Value
Langmuir	q_m (mg/g)	1071
	K_A (L/mg)	0.00699
	R^2_{adj}	0.953
Freundlich	K_B (mg/g)·(L/mg)$^{1/n}$	46.07
	n	1.96
	R^2_{adj}	0.877
Temkin	B(J/mol)	8.233
	K_C (L/g)	0.053
	R (J/mol·k)	8.314
	T (K)	298
	R^2_{adj}	0.967
Hill	q_m (mg/g)	846.1
	C	77.6
	n	1.86
	R^2_{adj}	0.997

Where K_A (L/mg) is the adsorption constants of Langmuir, C (mg/L) is the remaining concentration of mercury ions. R_A can be used to determine the feasibility of the adsorbent, and when $R_A > 1$, it means that adsorption is unfavorable, when $0 < R_A < 1$, indicating that adsorption is favorable. The calculated value of R_A was in the range of 0.3–0.79, indicating that adsorption was favorable.

3.5. Thermodynamic experiment

Chemical reaction was usually accompanied by energy change, therefore, in order to investigate whether the adsorption process of Zn-AHMT was endothermic or exothermic, this study was verified at 298 K, 308 K and 318 K, respectively. The variation of adsorption capacity with temperature is shown in Fig. 5. The relevant parameters were calculated and shown in Table 4. The thermodynamic calculation formulas were as follow Formula S3.

According to the experimental data, the adsorption capacity gradually decreased with the increase of temperature, and the fitting degree of lnK-1/T was 0.969, indicating that Zn-AHMT had better adsorption effect at low temperature. In addition, the values of δG and δH in the adsorption process were all negative by calculation. Based on the above analysis, it could be concluded that the adsorption process of adsorbent was a spontaneous and exothermic process.

3.6. Selective and renewability experiments

In fact, wastewater was composed of multiple ions, so it was necessary to study whether Zn-AHMT still had a strong affinity for Hg (II) under such conditions. This study was performed using laboratory simulated wastewater, and the corresponding experimental results were shown in Fig. 6(a). It could be seen that the concentration of Hg (II) in the solution changed the most before and after adsorption, decreasing from 99.97 mg/L to 0.23 mg/L, while the concentration of other metal ions did not change significantly, indicating that Zn-AHMT had a good affinity for Hg (II) even in the water where a variety of ions coexist. Based on the theory of hard and soft acid base, Hg (II) belonged to soft metal ions and Zn-AHMT contained a large number of soft bases such as N, S atoms, which had a strong affinity for Hg (II) [33]. Therefore, in the wastewater with the coexistence of Cr, Al, Mg, Mn, Co and Ni, Zn-AHMT could be highly selective for Hg (II). In addition, the distribution coefficient (K) could also be used to determine the affinity of Zn-AHMT to Hg (II). The value of the distribution coefficient reflected the degree of difficulty for adsorbent to adsorb metal ions. The higher the value was, the easier the adsorbent was to adsorb metal ions; otherwise, it was not easy to adsorb.

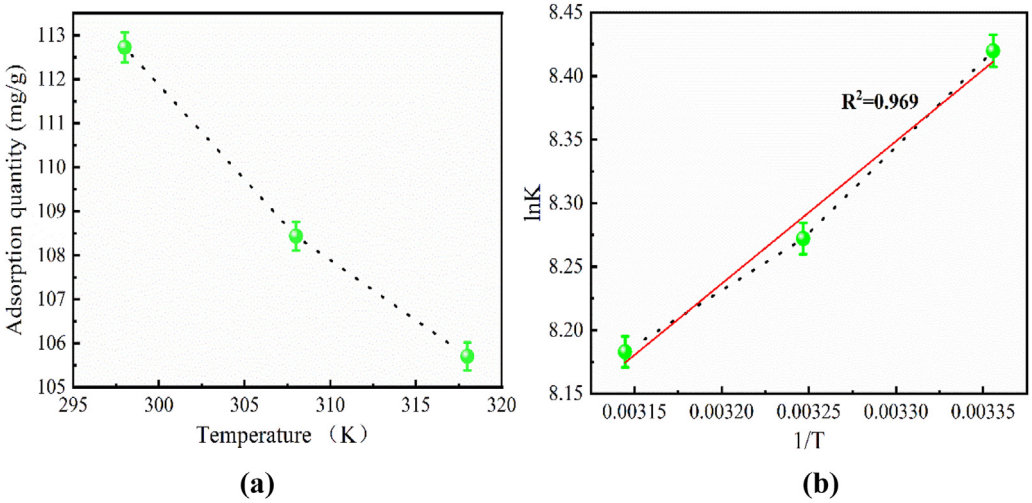

Fig. 5. Effect of temperature on adsorption capacity(a), lnK-1/T(b).

Table 4
Thermodynamic parameter.

T (K)	Q_e (mg/g)	Ke (mL/g)	δG (kJδmol^{-1})	δS (kJδmol$^{-1}\delta$K^{-1})	δH (kJδmol^{-1})
298	112.73	4536.22	-20.8	0.039	-10.49
308	108.44	3913.21	-21.2		
318	105.71	3579.58	-21.6		

The calculation formula was as follows:

$$K = \frac{Q_e}{C_e} \tag{4}$$

Where Q_e represents the adsorption capacity at equilibrium (mg/g), C_e represents the residual ion concentration (mg/L).

The results of the calculation were displayed in Table 5. The distribution coefficient of mercury ions was 433.6, which was much larger than other ions, suggesting that Zn-AHMT was easier to adsorb mercury ions. The results of two analyses showed that the affinity of Zn-AHMT to Hg (II) was greater than that of coexisting ions, which was sufficient to indicate that Zn-AHMT was selective.

Besides, reproducibility was also an attractive bright spot for adsorbents, which could greatly reduce the investment cost, so repeatable adsorbents had a wide range of application prospects in practical engineering. The reproducibility of Zn-AHMT was studied in this experiment, and the obtained experimental results were shown in Fig. 6(b). It could be seen that after five times of adsorption-desorption, the removal rate of Zn-AHMT could be maintained above 98%, indicating that Zn-AHMT had good stability.

Table 5
The relative parameters of ions.

Metal ions	Q_e (mg/g)	C_e (mg/L)	K (mL/g)
Hg	99.74	0.23	433.6
Ni	6.01	14.7	0.4088
Co	3.93	34.94	0.1124
Mn	0.85	30.3	0.028
Mg	0.11	25.87	0.0042
Al	0.34	25.41	0.0133
Cr	6.34	34.49	0.1838

3.7. Adsorption mechanism

Adsorption kinetics and isothermal experiments showed that the adsorption process of Zn-AHMT was chemisorption. To further explore

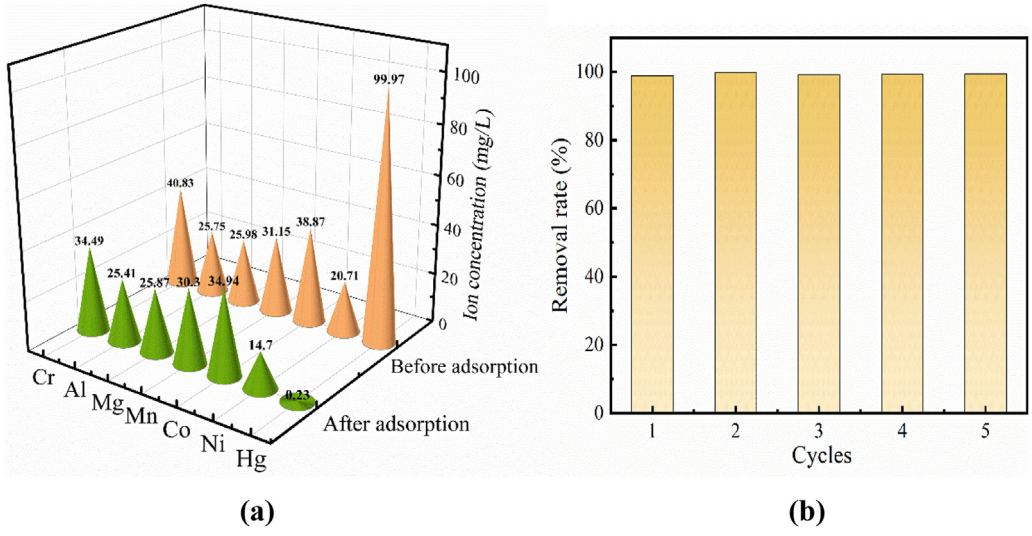

Fig. 6. Selectivity (a) and renewability (b) of Zn-AHMT.

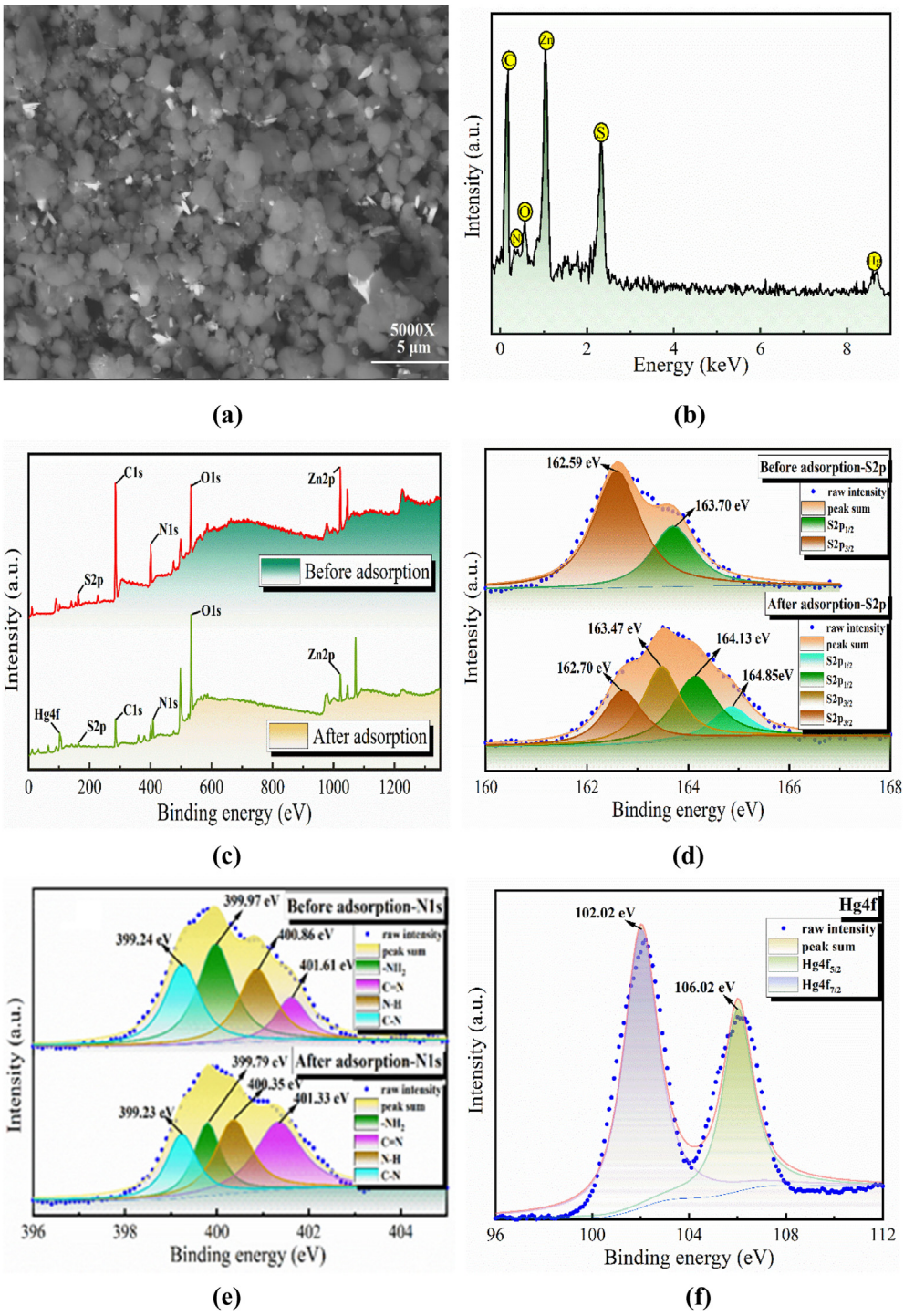

Fig. 7. The FESEM (a) and EDS (b) spectra of Zn-AHMT-Hg, survey peak spectrum (c),S2p (d), N1s (e) and Hg4f (f).

the adsorption mechanism, the adsorbents were analyzed in detail. The corresponding results were shown in Fig. 7. It could be clearly seen from the SEM (Fig. 7(a)) and EDS (Fig. 7(b)) spectra that Hg (II) were successfully adsorbed by Zn-AHMT, and the morphological characteristics of Zn-AHMT did not change significantly after adsorbing Hg (II), indicating Zn-AHMT had good stability in the adsorption process. By comparing the FTIR patterns of Zn-AHMT and Zn-AHMT-Hg, it was found that some peaks were shifted and new peaks appeared at 2437 cm-1, 2759 cm-1 and 2850 cm-1, which might be due to the reaction of functional groups on Zn-AHMT with mercury ions to form new complexes. Therefore, XPS analysis were applied to understand specifically which active sites of Zn-AHMT bound to Hg (II) to form complexes. Fig. 7(c) was the survey peak spectrum of Zn-AHMT before and after adsorption. The presence of Hg4f peak also indicated that mercury ions were adsorbed. The S2p and N1s patterns of Zn-AHMT and Zn-AHMT-Hg were shown in Fig. 7(d)–(e). It could be seen that the binding energies of $S2p_{1/2}$ and $S2p_{3/2}$ changed from 163.70 eV, 162.59 eV to 164.13 eV and 162.70 eV respectively before and after adsorption, and two new peaks appeared after adsorbing Hg (II), with the binding energies of 163.47 eV and 164.85 eV respectively [49]. 399.24 eV was the binding energy of C-N, 399.97 eV was the binding energy of $-NH_2$, and the binding energies of N-H and C═N were 400.86 eV and 401.61 eV, respectively [50,51]. After the adsorbent had

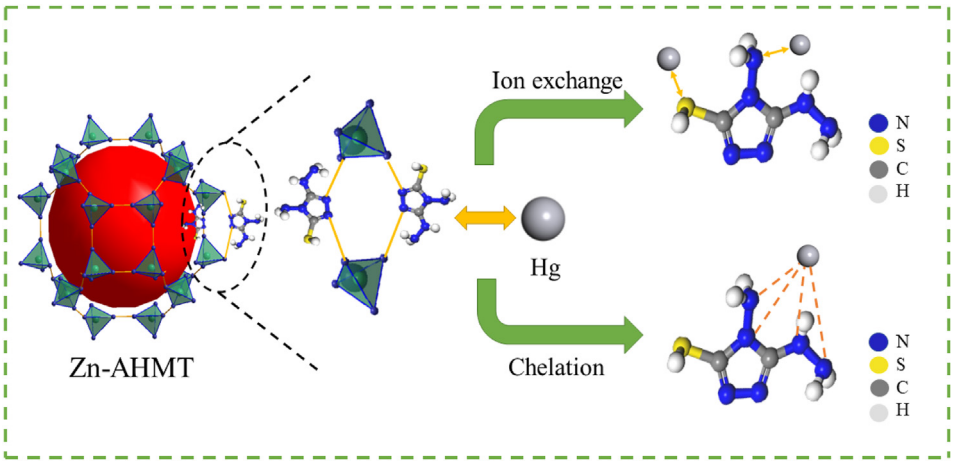

Fig. 8. Adsorption mechanism of Zn-AHMT.

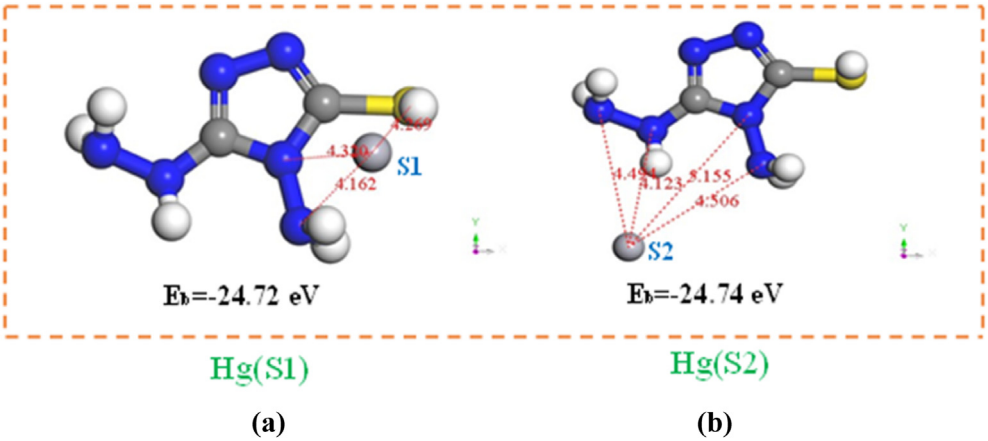

Fig. 9. The binding energies and bond distances of mercury ions with Zn-AHMT at different locations. (a) Hg(S1), (b) Hg(S2) (Sphere: White is H, Blue is N, Grey is C, Yellow is S).

completed the adsorption reaction, these binding energies had changed, indicating that some functional groups participate in the reaction during the adsorption process. In addition, the peak of Hg4f was also analyzed, and the results showed in Fig. 7(f) that the binding energies of $Hg4f_{7/2}$ and $Hg4f_{5/2}$ were 102.02 eV and 106.02 eV respectively [49]. Based on the above analysis and the theory of hard-soft-acid-base (HSAB) [52], it could be speculated that the change of most bond binding energies before and after adsorption was caused by the binding of -SH, $-NH_2$ and other active sites to Hg (II). And this interaction might be due to the ion exchange between Hg (II) and -SH, and chelation between Hg (II) and $-NH_2$. The adsorption mechanism was illustrated in Fig. 8.

3.8. DFT calculation and frontier molecular orbitals

To further explain the adsorption mechanism, the DFT calculation, a practical theoretical calculation tool, was used to provide accurate information about the energy of adsorption [53]. In this work, the Vienna ab Initio simulation package of DFT was used to evaluate possible stable geometry calculations. The geometric structure calculations were performed by Materials Studio 7.0. Simultaneously, both the Generalized Gradient Approximation (GGA) and Perdew-Burke-Ernzerhof (PBE) functions were used to estimate the exchange-correlation potential [54]. Based on the datasets, the mercury nitrate was used as Hg (II) model [14]. In addition, the HOMO-LUMO theory was also applied and the relevant calculation formulas were shown in Formula S4 [55].

In this work, two mercury ion sites (S1, S2) were selected to study the affinity of Zn-AHMT to Hg ions. As shown in Fig. 9, it could be found that when the mercury ion was at the S1 position (Fig. 9(a)), the bond distances of Hg-S and Hg-N were 4.269, 4.320 and 4.162 Å, and the associated binding energy (E_b) was -24.72 eV. While the Hg ion was at the S2 position in Fig. 9(b), the bond distances of Hg-N were 4.494, 4.123, 5.155 and 4.506 Å, and the corresponding binding energy (E_b) was -24.74 eV. There is small difference between the E_b(S1) and E_b(S2), indicating that Zn-AHMT had similar affinity for Hg ions in the two cases. However, the bonding (S2) is the preferred as $E_b(S2) < E_b(S1)$. Furthermore, the results of related parameters and the HOMO-LUMO diagrams were also displayed in Table 6 and Fig. 10, respectively. These parameters reflected the chemical properties of the complexes produced by the combination of Zn-AHMT and mercury ions under different conditions. As could be seen from Fig. 10(c-d), when Zn-AHMT and mercury ions bound at the S1 site, the E_H of the complex was -5.39 eV, E_L was -1.73 eV, and the HOMO-LUMO energy gap δE(S1) was 3.65 eV. When Zn-AHMT and mercury ions bound at the S2 site, the E_H of the complex was -5.29 eV, E_L was -1.49 eV, and the HOMO-LUMO energy gap δE(S2) was 3.80 eV. Because δE(S2) was larger than δE(S1) (Fig. 10(h)), the complex formed by the

Table 6
Calculation results of related parameters.

mercury ion site	δE (eV)	η (eV)	μ (eV))	ω (eV))
Hg(S1)	3.65	1.83	-3.56	3.47
Hg(S2)	3.80	1.90	-3.39	3.02

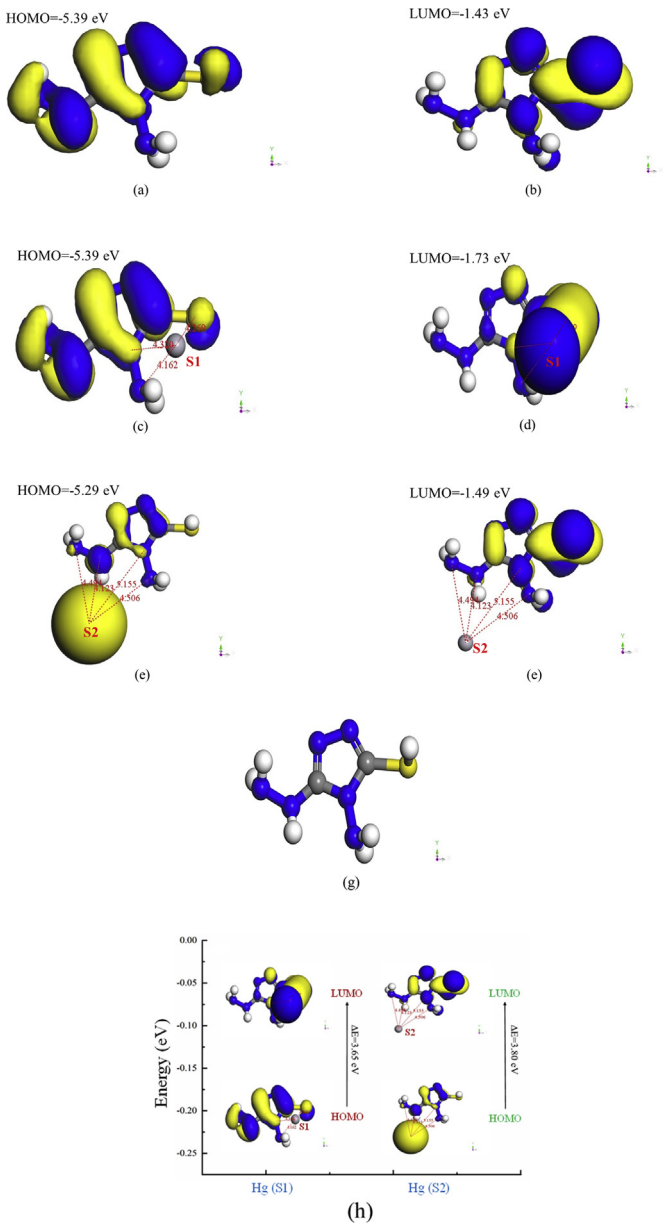

Fig. 10. The HOMO (a) and LUMO (b) diagram of monomer, the HOMO (c) and LUMO (d) diagram of Hg(S1), the HOMO (e) and LUMO (f) diagram of Hg(S2), monomer (g), energy gap diagram (h). (Sphere: White is H, Blue is N, Grey is C, Yellow is S).

second binding was more stable, which was consistent with the results of previous analysis. Besides, for the complex formed at the S1 site, HOMOs were mainly distributed on S and N atoms, while LUMOs were mainly distributed on mercury ions. On the contrary, HOMOs and LUMOs were mainly distributed on mercury ions and the S and N atoms of the complex formed at S2, respectively. Based on the above analysis, it could be concluded that Zn-AHMT was more likely to combine with mercury ions at the S2 position, and the complex formed was more stable, moreover, the S atom also had a better adsorption effect. That is to say, N and S atoms cooperate to complete the adsorption reaction.

4. Conclusion

The adsorbents were prepared by one-step method and characterized by FTIR, SEM and XRD. Batch experiment results showed that the adsorption capacity of Zn-AHMT could reach 802.8 mg/g under the optimal pH=3.0. Isothermal and kinetic experiments have confirmed that the reaction process of Zn-AHMT was chemisorption in accordance with Hill model and pseudo-second order model. Thermodynamic experiments showed that the adsorption process was spontaneous and exothermic. Selectivity and repeated experiment indicated that the adsorbent had a stronger affinity for mercury ions than other ions, and the removal rate was above 98% each time. The adsorption mechanism had been studied by XPS, DFT calculations, frontier molecular orbital theory and showed that the adsorption process was mainly caused by the chelation and ion exchange between Zn-AHMT and mercury ions. The adsorption reaction was the result of the synergistic action of S and N atoms, and the product with Hg-N bond was more stable than that of Hg-S during adsorption. In summary, it could be seen that Zn-AHMT had great potential to remove mercury ions.

Declaration of competing interest

None.

Acknowledgements

This work was supported by the Hubei Provincial Department of Education Science and Technology Research Program Young Talent Project (Q20201102) and the National Natural Science Foundation of China (51864042 and 51804220).

Appendix A. Supplementary data

Supplementary data to this article can be found online at https://doi.org/10.1016/j.nanoms.2021.06.005.

References

[1] R. Peng, G. Chen, F. Zhou, R. Man, J. Huang, Catalyst-free synthesis of triazine-based porous organic polymers for Hg^{2+} adsorptive removal from aqueous solution, Chem. Eng. J. 371 (2019) 260–266.
[2] Y. Huang, S. Xia, J. Lyu, J. Tang, Highly efficient removal of aqueous Hg^{2+} and $CH3Hg^{+}$ by selective modification of biochar with 3-mercaptopropyltrimethoxysilane, Chem. Eng. J. 360 (2019) 1646–1655.
[3] G. Lin, C. Wang, X.T. Li, Y.H. Xi, W. Wang, L.B. Zhang, J. Chang, Synthesis of coordination polymer by 2,2′-dithiodipropionic acid and selective removal of Hg(ii)/Pb(ii) in wastewater[J], J. Taiwan Inst. Chem. E 113 (2020) 315–324.
[4] A. Sari, M. Tuzen, Removal of mercury(II) from aqueous solution using moss (Drepanocladus revolvens) biomass: equilibrium, thermodynamic and kinetic studies, J. Hazard Mater. 171 (2009) 500–507.
[5] N. Salandari-Jolge, A.A. Ensafi, B. Rezaei, Ultra-sensitive electrochemical aptasensor based on zeolitic imidazolate framework-8 derived Ag/Au core-shell nanoparticles for mercury detection in water samples, Sensor. Actuator. B Chem. 331 (2021) 129426.
[6] A. Labidi, A.M. Salaberria, J. Labidi, M. Abderrabba, Preparation of novel carboxymethylchitosan-graft-poly(methylmethacrylate) under microwave irradiation as a chitosan-based material for Hg^{2+} removal, Microchem. J. 148 (2019) 531–540.
[7] Y. Wan, D. Zou, Y. Cui, Y. Yang, G. Qian, A Zn based anionic metal-organic framework for trace Hg^{2+} ion detection, J. Solid State Chem. 266 (2018) 70–73.
[8] R. Vinodh, R. Padmavathi, D. Sangeetha, Separation of heavy metals from water samples using anion exchange polymers by adsorption process, Desalination 267 (2011) 267–276.
[9] M. Arshadi, Manganese chloride nanoparticles: a practical adsorbent for the sequestration of Hg(II) ions from aqueous solution, Chem. Eng. J. 259 (2015) 170–182.
[10] Y. Gan, G. Chen, Y. Sang, F. Zhou, R. Man, J. Huang, Oxygen-rich hyper-cross-linked polymers with hierarchical porosity for aniline adsorption, Chem. Eng. J. 368 (2019) 29–36.
[11] F. Ke, J. Jiang, Y. Li, J. Liang, X. Wan, S. Ko, Highly selective removal of Hg^{2+} and Pb^{2+} by thiol-functionalized Fe_3O_4@metal-organic framework core-shell magnetic microspheres, Appl. Surf. Sci. 413 (2017) 266–274.
[12] F. Ke, L.G. Qiu, Y.P. Yuan, F.M. Peng, X. Jiang, A.J. Xie, Y.H. Shen, J.F. Zhu, Thiol-functionalization of metal-organic framework by a facile coordination-based postsynthetic strategy and enhanced removal of Hg^{2+} from water, J. Hazard Mater. 196 (2011) 36–43.
[13] X.L. Liu, H.W. Pang, X.W. Liu, Q. Li, N. Zhang, L. Mao, M.Q. Qiu, B.W. Hu, H. Yang, X.K. Wang, Orderly porous covalent organic frameworks-based materials: superior adsorbents for pollutants removal from aqueous solutions, Innovation 2 (2021) 100076.

[14] M. Zhao, Z. Huang, S. Wang, L. Zhang, Y. Zhou, Design of l-cysteine functionalized UiO-66 MOFs for selective adsorption of Hg(II) in aqueous medium, ACS Appl. Mater. Interfaces 11 (2019) 46973–46983.
[15] S. Mokhtari, H. Faghihian, Modification of activated carbon by 2,6-diaminopyridine for separation of Hg^{2+} from aqueous solutions, J. Environ. Chem. Eng. 3 (2015) 1662–1668.
[16] A.M. Donia, A.A. Atia, K.Z. Elwakeel, Selective separation of mercury(II) using magnetic chitosan resin modified with Schiff's base derived from thiourea and glutaraldehyde, J. Hazard Mater. 151 (2008) 372–379.
[17] K.D. Zhang, F.C. Tsai, N. Ma, Y. Xia, H.L. Liu, X.Q. Zhan, X.Y. Yu, X.Z. Zeng, T. Jiang, D. Shi, C.J. Chang, Adsorption behavior of high stable Zr-based MOFs for the removal of acid organic dye from water, Materials 10 (2017) 205.
[18] Z. Ding, W. Yang, K. Huo, L. Shaw, Thermodynamics and kinetics tuning of LiBH4 for hydrogen storage[J], Prog. Chem. (2021), https://doi.org/10.7536/PC200831.
[19] A. Huang, Q. Liu, N. Wang, J. Caro, Organosilica functionalized zeolitic imidazolate framework ZIF-90 membrane for CO_2/CH_4 separation, Microporous Mesoporous Mater. 192 (2014) 18–22.
[20] G. Lin, H.T. Qu, T.F. Xie, L.K. Gu, J. Liu, S.X. Wang, W. Wang, L.B. Zhang, T. Wang, H.K. Di, J. Chang, C. Srinivasakannan, Roles of tannic acid and gelatin in Zn electrowinning and their inhibition mechanisms investigated via electrochemical methods[J], Hydrometallurgy 195 (2020) 105390.
[21] J. Liu, P.K. Thallapally, B.P. McGrail, D.R. Brown, J. Liu, Progress in adsorption-based CO2 capture by metal–organic frameworks, Chem. Soc. Rev. 41 (2012) 2308–2322.
[22] L. Huang, M. He, B. Chen, B. Hu, A designable magnetic MOF composite and facile coordination-based post-synthetic strategy for the enhanced removal of Hg^{2+} from water, J. Mater. Chem. A 3 (2015) 11587–11595.
[23] Z. Ding, S. Li, Y. Zhou, Z. Chen, W. Yang, W. Ma, L. Shaw, $LiBH_4$ for hydrogen storage - new perspectives, Nano Mater. Sci. 2 (2020) 109–119.
[24] M. Kim, J.F. Cahill, Y. Su, K.A. Prather, S.M. Cohen, Postsynthetic ligand exchange as a route to functionalization of 'inert' metal–organic frameworks, Chem. Sci. 3 (2012) 126–130.
[25] Q.L. Zhu, Q. Xu, Metal-organic framework composites, Chem. Soc. Rev. 43 (2014) 5468–5512.
[26] L. Huang, M. He, B. Chen, B. Hu, Magnetic Zr-MOFs nanocomposites for rapid removal of heavy metal ions and dyes from water, Chemosphere 199 (2018) 435–444.
[27] X. Luo, L. Ding, J. Luo, Adsorptive removal of Pb(II) ions from aqueous samples with amino-functionalization of metal–organic frameworks MIL-101(Cr), J. Chem. Eng. Data 60 (2015) 1732–1743.
[28] L. Jiang, W. Zhang, C. Luo, D. Cheng, J. Zhu, Adsorption toward trivalent rare earth element from aqueous solution by zeolitic imidazolate frameworks, Ind. Eng. Chem. Res. 55 (2016) 6365–6372.
[29] Z. Chang, F. Li, X. Qi, B. Jiang, J. Kou, C. Sun, Selective and efficient adsorption of Au(III) in aqueous solution by Zr-based metal-organic frameworks (MOFs): an unconventional way for gold recycling, J. Hazard Mater. 391 (2020) 122175.
[30] Z. Huang, M. Zhao, C. Wang, S. Wang, L. Dai, L. Zhang, Preparation of a novel Zn(II)-Imidazole framework as an efficient and regenerative adsorbent for Pb, Hg, and as ion removal from water, ACS Appl. Mater. Interfaces 12 (2020) 41294–41302.
[31] G. Lin, S. Wang, L. Zhang, T. Hu, S. Cheng, L. Fu, C. Xiong, Enhanced and selective adsorption of Hg(2+) to a trace level using trithiocyanuric acid-functionalized corn bract, Environ. Pollut. 244 (2019) 938–946.
[32] J.A. Antunes, T.A. de Toledo, L.E. da Silva, P.T.C. Freire, A.M.R. Teixeira, H.D.M. Coutinho, J.L.B. Faria, R.J. Ramos, R.R.F. Bento, Characterization of zinc complex with 4-{[(1E)-(2 Hydroxyphenyl) methylidene]amino}-1,5-dimethyl-2-phenyl-1,2-dihydro-3H-pyrazol-3-one by FT-IR and FT-Raman spectroscopies and DFT calculations, J. Mol. Struct. 1202 (2020) 127295.
[33] G. Lin, T. Hu, S. Wang, T. Xie, L. Zhang, S. Cheng, L. Fu, C. Xiong, Selective removal behavior and mechanism of trace Hg(II) using modified corn husk leaves, Chemosphere 225 (2019) 65–72.
[34] M.Q. Qiu, Z.X. Liu, S.Q. Wang, B.W. Hu, The photocatalytic reduction of U(VI) into U(IV) by ZIF-8/g-C3N4 composites at visible light, Environ. Res. 196 (2021) 110349.
[35] S. Cheng, B. Xing, C. Shi, Y. Nie, H. Xia, Efficient and selective removal of Pb(II) from aqueous solution by modification crofton weed: experiment and density functional theory calculation, J. Clean. Prod. 280 (2021) 124407.
[36] A. Gunay, E. Arslankaya, I. Tosun, Lead removal from aqueous solution by natural and pretreated clinoptilolite: adsorption equilibrium and kinetics, J. Hazard Mater. 146 (2007) 362–371.
[37] M. Al-Harahsheh, R. Shawabkeh, A. Al-Harahsheh, K. Tarawneh, M.M. Batiha, Surface modification and characterization of Jordanian kaolinite: application for lead removal from aqueous solutions, Appl. Surf. Sci. 255 (2009) 8098–8103.
[38] M.A.J. Mazumder, M.T. Alhaffar, S.A. Ali, Immobilization of two polyelectrolytes leading to a novel hydrogel for high-performance Hg^{2+} removal to ppb and sub-ppb levels, Chem. Eng. J. 334 (2018) 1440–1454.
[39] Z.K.L. Lin, Y.W. Hu, Y.J. Yuan, B.W. Hu, B.L. Wang, Comparative analysis of kinetics and mechanisms for Pb(II) sorption onto three kinds of microplastics, Ecotoxicol. Environ. Saf. 208 (2021) 111451.
[40] Y. Shen, X. Zhao, X. Zhang, S. Li, D. Liu, L. Fan, Removal of Cu^{2+} from the aqueous solution by tartrate-intercalated layered double hydroxide, Desalin, Water Treat. 57 (2016) 2064–2072.
[41] C. Wang, G. Lin, J. Zhao, S. Wang, L. Zhang, Y. Xi, X. Li, Y. Ying, Highly selective recovery of Au(III) from wastewater by thioctic acid modified Zr-MOF: experiment and DFT calculation, Chem. Eng. J. 380 (2020) 122511.
[42] S. Cheng, L. Zhang, H. Xia, S. Zhang, J. Peng, S. Wang, Crofton weed derived activated carbon by microwave-induced KOH activation and application to wastewater treatment, J. Porous Mater. 23 (2016) 1597–1607.
[43] B. Li, Y. Zhang, D. Ma, Z. Shi, S. Ma, Mercury nano-trap for effective and efficient removal of mercury(II) from aqueous solution, Nat. Commun. 5 (2014) 5537.
[44] D. Xu, W.D. Wu, H.J. Qi, R.X. Yang, W.Q. Deng, Sulfur rich microporous polymer enables rapid and efficient removal of mercury(II) from water, Chemosphere 196 (2018) 174–181.
[45] X. Luo, T. Shen, L. Ding, W. Zhong, J. Luo, S. Luo, Novel thymine-functionalized MIL-101 prepared by post-synthesis and enhanced removal of Hg(2+) from water, J. Hazard Mater. 306 (2016) 313–322.
[46] T.A. Saleh, Isotherm, kinetic, and thermodynamic studies on Hg(II) adsorption from aqueous solution by silica- multiwall carbon nanotubes, Environ. Sci. Pollut. Res. Int. 22 (2015) 16721–16731.
[47] N. Caner, A. Sarı, M. Tüzen, Adsorption characteristics of mercury(II) ions from aqueous solution onto chitosan-coated diatomite, Ind. Eng. Chem. Res. 54 (2015) 7524–7533.
[48] A. Santhana Krishna Kumar, S.-J. Jiang, Preparation and characterization of exfoliated graphene oxide–l-cystine as an effective adsorbent of Hg(ii) adsorption, RSC Adv. 5 (2015) 6294–6304.
[49] H. Yang, C. Peng, J. Han, Y. Song, L. Wang, Three-dimensional macroporous Carbon/Zr-2,5-dimercaptoterephthalic acid metal-organic frameworks nanocomposites for removal and detection of Hg(II), Sensor. Actuator. B Chem. 320 (2020) 128447.
[50] Y. Fu, Y. Sun, Y. Zheng, J. Jiang, C. Yang, J. Wang, J. Hu, New network polymer functionalized magnetic-mesoporous nanoparticle for rapid adsorption of Hg(II) and sequential efficient reutilization as a catalyst, Separ. Purif. Technol. 259 (2021) 118112.
[51] J. Tang, J. Zhao, S. Wang, L. Zhang, M. Zhao, Z. Huang, Y. Hu, Pre-modification strategy to prepare a novel Zr-based MOF for selective adsorption of Palladium(II) from solution, Chem. Eng. J. (2020) 127223.
[52] A. Alfarra, E. Frackowiak, F. Béguin, The HSAB concept as a means to interpret the adsorption of metal ions onto activated carbons, Appl. Surf. Sci. 228 (2004) 84–92.
[53] I. Matrane, M. Mazroui, Y. Boughaleb, Diffusion and adsorption of Au and Pt adatoms on ideal and missing row reconstructed surfaces of Au(110): DFT and EAM calculations, Surf. Sci. 677 (2018) 83–89.
[54] C. Xiong, S. Wang, P. Hu, L. Huang, C. Xue, Z. Yang, X. Zhou, Y. Wang, H. Ji, Efficient selective removal of Pb(II) by using 6-aminothiouracil-modified Zr-based organic frameworks: from experiments to mechanisms, ACS Appl. Mater. Interfaces 12 (2020) 7162–7178.
[55] S. Kaviani, S. Shahab, M. Sheikhi, M. Ahmadianarog, DFT study on the selective complexation of meso-2,3-dimercaptosuccinic acid with toxic metal ions (Cd^{2+}, Hg^{2+} and Pb^{2+}) for pharmaceutical and biological applications, J. Mol. Struct. 1176 (2019) 901–907.